Improved Modelling of Milky Way Dark Matter Halo

A PROJECT REPORT

Session Jan'15-Apr'15

CENTRE *for* EXCELLENCE IN BASIC SCIENCES
Department of Atomic Energy
University of Mumbai, Kalina campus
Mumbai - 400098, India

Author:
S Vivekanandji Chaurasia
Roll No:
P011506

Guide:
Prof. Subhabrata Majumdar
Department of Theoretical Physics
TIFR-Mumbai

Abstract

The correct modelling of the phase-space of Dark Matter (DM) in our galaxy, in presence of other visible mass components, is of crucial importance in cosmology and DM detection experiments. Using current and upcoming rotation curve measurements, we present an improved and robust measurement of the DM distribution in our Galaxy. We make use of different DM distribution models, observationally motivated visible matter (VM) priors and do a full Monte Carlo Markov Chain exploration of the joint DM+VM model of our Milky Way. We provide tight constraints on the density of DM in the solar neighborhood and the scale length of the Milky Way DM halo. Although current observations cannot differentiate between different models of DM distribution, we show that upcoming data, from mission like GAIA, will be able to nail down the DM distribution with exquisite accuracy.

Acknowledgements

This report was written as part of my VIIIth semester project offered by the Physics department at UM-DAE CBS, which I took under the supervision of Prof. Subhabrata Majumdar. I am extremely grateful for his guidance and insight. I would also like to thank Sebastian Seehars and Digvijay Wadekar for providing me technical help with getting the mcmc running and analysing it.

Contents

1 The galaxy rotation problem

In 1975, Vera Rubin, an astronomer at the Department of Terrestrial Magnetism at the Carnegie Institution of Washington together with her colleague Kent Ford, discovered that most stars in spiral galaxies orbit at roughly the same speed. [1]This implied that the galaxy masses grow approximately linearly with radius well beyond the location of most of the stars (the galactic bulge).

They presented their results in an influential paper in 1980. [2] These were the first robust results to suggest that either Newtonian gravity does not apply universally or more than 50% of the mass of the galaxies was contained in the relatively dark galactic halo. Although initially met with skepticism, Rubin's results have been confirmed over the subsequent decades. [3]

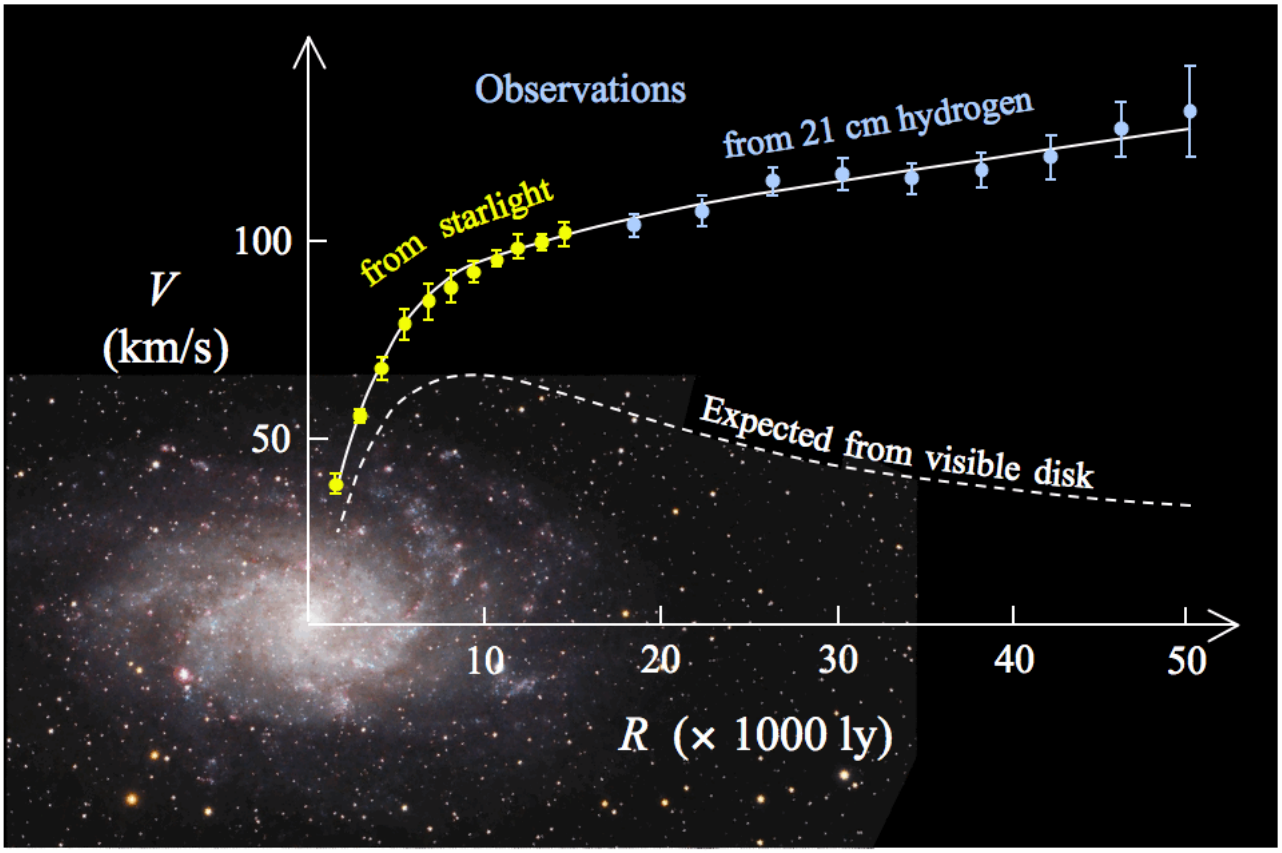

Figure 1: Rotation curve for M33

When we apply Newtonian mechanics and assume that most of the mass(visible) of the galaxy to be in the galactic bulge near the center(as was thought to be!), matter (such as stars and gas) in the disk portion of a spiral should orbit the center of the galaxy in a similar way as the planets orbit the Sun in the solar system, i.e. the average orbital speed of an object at a specified distance away from the majority of the mass distribution would decrease inversely with the square root of the radius of the orbit(the dashed line in Fig.[1]).

$$\frac{m_* v_{circ}^2}{r} = \frac{GMm_*}{r^2} \tag{1}$$

$$i.e;\ v_{circ}(r) = \sqrt{\frac{GM}{r}}\ (theoretically)$$

$$but\ observationally:\ v_{circ}(r) \approx constant \tag{2}$$

$$\implies M(r) \propto r \tag{3}$$

However, observations of the rotation curve of spiral galaxies do not show this feature. Rather than decreasing in the inverse square root relationship as expected, the curves are "flat", i.e. outside of the central bulge the speed is nearly a constant (the solid line in Fig.[1]). It is also observed that galaxies with a uniform distribution of luminous matter have a rotation curve that slopes up from the center to the edge, and most low-surface-brightness galaxies (LSB galaxies) rotate with a rotation curve that slopes up from the center, indicating little core bulge.

These features of the rotation curve can be explained if one concocts a substantial amount of matter permeating the galaxy that is not emitting light in the mass-to-light ratio of the central bulge. This non-luminous extra mass was dubbed, "*dark matter*". Its existence was first proposed in the 1930s by Jan Oort in his measurements of the Oort constants and by Fritz Zwicky in his studies of the masses of galaxy clusters, though these proposals were left unexplored until after Rubin's work was accepted as correct. The existence of non-baryonic cold dark matter (**CDM**) is today a major feature of the ΛCDM model that describes the cosmology of the universe.

2 Modelling spiral galaxies

One can view galaxies as large systems of interacting objects such as stars and gas clouds. Since typical galaxies contain of the order of 10^{11} stars, it is not practical to analyse all possible two-body interactions in such a system. Instead, one treats the mass distribution of a galaxy as a continuous quantity and therefore determines the gravitational effects in a macroscopic(averaged-out) fashion, that is, by considering the integral effects of matter on a test mass. A spiral galaxy is therefore modelled as a superposition of visible matter and dark matter mass distributions in order to explain the observed rotation curves. In this section we will discuss the nature of the density profiles and the corresponding potentials arising from continuous but finite distributions of matter. A spiral galaxy is modelled with three components, the central *bulge* of the visible matter, the *disk* of the visible matter and the spherical *dark matter halo*.

2.1 Dark matter density profiles

a.) **NFW Profile**
The Navarro-Frenk-White profile or NFW profile is a spatial mass distribution of dark matter fitted to dark matter haloes identified in N-body simulations by Julio Navarro, Carlos Frenk and Simon White. The NFW profile is one of the most commonly used model profiles for dark matter halos. This, when normalised to DM density at solar

location, $\rho_{DM,\circ}$ is given by:

$$\rho_{NFW}(r) = \rho_{DM,\circ}\left(\frac{R_0}{r}\right)\left(\frac{r_s + R_0}{r_s + r}\right)^2 \tag{4}$$

b.) **Burkert Profile**
The Burkert profile is a cored profile that appears to provide a good fit to the DM distribution and when normalized to DM density at solar location, $\rho_{DM,\circ}$ is given by:

$$\rho_{Bur}(r) = \frac{\rho_{DM,\circ}(r_s + R_0)(r_s^2 + R_0^2)}{(r_s + r)(r_s^2 + r^2)} \tag{5}$$

c.) **Einasto Profile**
The Einasto profile is as good a fit as the NFW profile, if not better, to simulate galaxy-sized dark matter halos and this when normalized to DM density at solar location, $\rho_{DM,\circ}$ is given by:

$$\rho_{Ein}(r) = \rho_{DM,\circ}\ \exp\left(-\frac{2}{\gamma}\left[\left(\frac{r}{r_s}\right)^{\gamma} - \left(\frac{R_0}{r_s}\right)^{\gamma}\right]\right) \tag{6}$$

Where R_0 is the distance of the sun from the Galactic centre. These profiles have two free parameters, namely, the density $\rho_{DM,\circ}$ and the scale radius r_s. We will fix $\gamma = 0.17$ for our purpose.

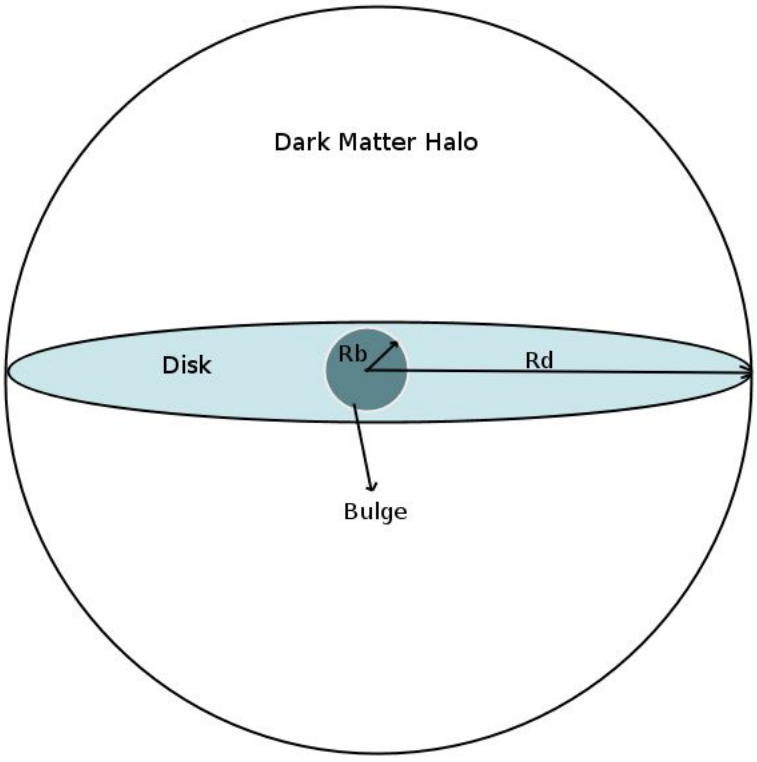

Figure 2: schematic of our model

2.2 Visible matter density profiles

The visible matter distribution can be effectively modelled[4] in terms of a spheroidal bulge superposed on an axisymmetric disk(Fig.[2]). The corresponding density distribution for the

bulge is:

$$\rho_b(r) = \rho_{b0}\left(1 + \left(\frac{r}{r_b}\right)^2\right)^{-\frac{3}{2}} \tag{7}$$

where the parameters ρ_{b0} and r_b are the central density and the scale radius of the bulge. The disk has a mass distribution as given by:

$$\rho_d(R,z) = \frac{\Sigma_\circ}{2z_d}\ e^{-(R-R_0)/R_d}\ e^{-|z|/z_d} \tag{8}$$

where R and z are the axisymmetrical coordinates, R_d and z_d are the scale length and scale height of the disk, respectively, and $\Sigma_\circ$ is its local surface density.

2.3 Potentials

Given a mass distribution(ρ) one can find the gravitational potential(Φ) by solving the respective Poisson's equation:

$$\nabla^2\Phi = 4\pi G\rho \tag{9}$$

For the case of spherically symmetric mass distributions the potential can be analytically calculated as:

Dark Matter Halo:

$$M(r) = \int_0^r 4\pi r'^2\ \rho_{DM}(r')\ dr' \tag{10}$$

a.) NFW-potential

$$M(r) = 4\pi\ \rho_{DM,\circ}\ R_0(r_s+R_0)^2\ \left\{ln\left(\frac{r_s+r}{r_s}\right) + \frac{r_s}{r_s+r} - 1.\right\} \tag{11}$$

b.) Burkert-potential

$$M(r) = \pi\ \rho_{DM,\circ}(R_0+r_s)(r_s^2+R_0^2)\left\{-2\tan^{-1}\left(\frac{r}{r_s}\right) + 2ln\left(\frac{r_s+r}{r_s}\right) + ln\left(\frac{r_s^2+r^2}{r_s^2}\right)\right\} \tag{12}$$

c.) Einasto-potential

$$M(r) = 4\pi\ \rho_{DM,\circ}e^{\frac{2}{\gamma}\left(\frac{R_0}{r_s}\right)^\gamma}\left[\left(\frac{\gamma}{2}\right)^{1/\gamma} r_s\right]^3 \frac{1}{\gamma}\Gamma\left(\frac{3}{\gamma}\right)\left[1. - \frac{\Gamma\left(\frac{3}{\gamma}, \frac{2}{\gamma}\left(\frac{r}{r_s}\right)^\gamma\right)}{\Gamma\left(\frac{3}{\gamma}\right)}\right] \tag{13}$$

Where $\Gamma(a,x) = \int_x^\infty e^{-t}t^{a-1}\ dt$ is the incomplete gamma function.

Now the potential can simply be written as:

$$\Phi(r) = \frac{GM(r)}{r} \tag{14}$$

Bulge:

Similar to above, we can write the potential due to the bulge with mass as a function of radius given by:

$$M(r) = 4\pi\ \rho_{b0} \left\{ \sinh^{-1}\left(\frac{r}{r_b}\right)\ r_b^3 - \frac{r\ \sqrt{1+(\frac{r}{r_b})^2}\ r_b^4}{r^2+r_b^2} \right\} \tag{15}$$

Disk:

Calculating the potential for the disk is not as trivial as for the spherical symmetry case. The disk has a cylindrical symmetry and has a finite boundary giving rise to boundary conditions. We have to try to compute the potential by directly solving Poisson's equation(or the Laplace's equation) with proper boundary conditions. If one can compute the expression for the potential analytically then that will give an advantage over numerically solving the Poisson's equation. Computation from analytical expressions is faster(much faster!) than numerically solving the equations.

Typical galaxies such as the Milky Way are characterized by cylindrical disks that are very thin compared to the disk radii. Therefore, to first order we will ignore their thickness for mathematical simplicity . We therefore consider a circular disk of zero thickness characterized by some surface density distribution, $\Sigma(R) = \Sigma_\circ\ e^{-(R-R_0)/R_d}$, where R is the radial distance from the center of the disk Fig.[3].

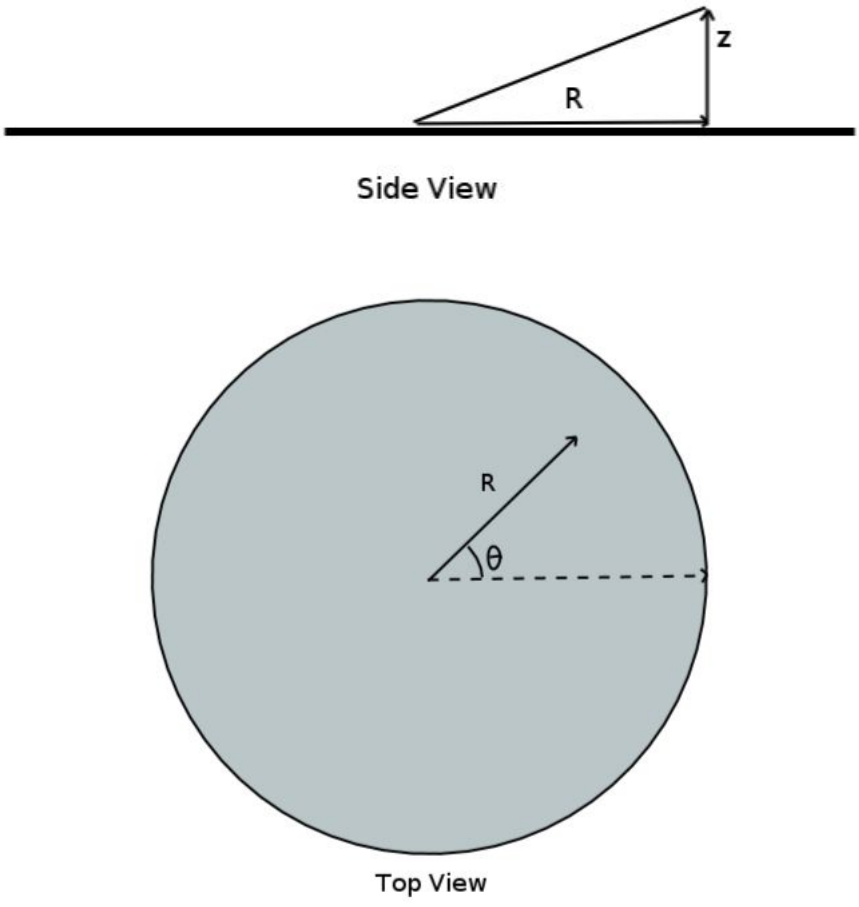

Figure 3: cross-section of the galaxy

Since the disk is infinitely thin we can start with the Laplace equation rather than the Poisson equation and we expect that the resulting solution would be valid for all regions outside the disk. Since the disk has cylindrical symmetry and since we want a solution for all 3D space we write the Laplace equation in cylindrical coordinates.

$$\nabla^2\Phi = \frac{1}{R}\frac{\partial}{\partial R}\left(\frac{1}{R}\frac{\partial\Phi}{\partial R}\right) + \frac{\partial^2\Phi}{\partial z^2} = 0 \tag{16}$$

Using separation of variables, we look for a solution of the form

$$\Phi(R,z) = J(R)\ Z(z)$$

Substituting into the Laplace equation, we get

$$\frac{1}{J(R)}\frac{1}{R}\frac{d}{dR}\left(R\frac{dJ}{\partial R}\right) = -\frac{1}{Z(z)}\frac{\partial^2 Z}{\partial z^2} = -k^2$$

The solution to this equation can be found in any advanced astrophysics textbook.[5] We can write the final form of the potential with the assumption of the thin disk as:

$$\Phi(R,z=0) = -2\pi G\Sigma_0 R_d^2 e^{R_0/R_d}\int_0^\infty dk\frac{J_0(kR)}{[1+(kR_d)^2]^{3/2}} \tag{17}$$

Solving the above integral, we get

$$\Phi(R,z=0) = -\pi G\Sigma_0 R_d^2 e^{R_0/R_d} R\left\{I_0\left(\frac{R}{2R_d}\right)K_0\left(\frac{R}{2R_d}\right) - I_1\left(\frac{R}{2R_d}\right)K_1\left(\frac{R}{2R_d}\right)\right\} \tag{18}$$

Where I_0 and I_1 are the modified Bessel functions of the first kind and of order 0 and 1 respectively. Similarly, K_0 and K_1 are modified Bessel functions of the second kind and of order 0 and 1 respectively.

2.4 Rotation velocity

For a given set of Galactic model parameters, the rotation speed, $v_c(r)$ is given by:

$$v_c^2(r) = r\frac{\partial}{\partial r}\left[\Phi_{DM}(r,z=0) + \Phi_{VM}(r,z=0)\right] \tag{19}$$

Particularly, for spherical mass distribution the contribution to the rotation speed can be written as

$$v_c^2(r) = G\frac{M(r)}{r} \tag{20}$$

and due to the disk it is:

$$v_c^2(r) = 4\pi G\Sigma_0 R_d\left(\frac{r}{2R_d}\right)^2 e^{\frac{R_0}{R_d}}\left\{I_0\left(\frac{R}{2R_d}\right)K_0\left(\frac{R}{2R_d}\right) - I_1\left(\frac{R}{2R_d}\right)K_1\left(\frac{R}{2R_d}\right)\right\} \tag{21}$$

3 Link between MCMC, the RC data, and the model parameters

Various models describe the dark matter distribution in galaxies. Each model is based on its own specific geometry and has its own set of parameters, characterising the dark matter properties. The MCMC approach aims to study quantitatively how the existing (or future) rotation curve(RC) measurements can constrain these models or, equivalently, how in such models the set of parameters (and their uncertainties) can be inferred from the data.

In our study, the set of parameters that are used in modelling the rotation curve data are $\rho_{DM\circ}$, r_S, ρ_{b0}, r_b, $\Sigma_\circ$ and R_d (6D-parameter space). These model parameters are constrained such as to reproduce the measured rotation curve. The "goodness" of fit to the data is done by the χ^2 test-statistics. Assuming the χ^2 statistics is applicable to the problem at stake, confidence intervals in these parameters can be extracted. In particular, we compute $\chi^2 \equiv \Sigma_{i=1}^{i=N} \left(\frac{v^i_{c,obs} - v^i_{c,th}}{v^i_{c,error}} \right)$, where $v^i_{c,obs}$ and $v^i_{c,error}$ are, respectively, the observational value of the circular rotation speed and its error at the i^{th} value of the galactocentric distance, and $v^i_{c,th}$ is the corresponding theoretically calculated circular rotation speed.

The main drawback of this approach is the computing time required to extend the calculation of the χ^2-surface to a wider parameter space. This is known as the curse of dimensionality, due to the exponential increase in volume associated with adding extra dimensions to the parameter space, while the good regions of this space (for instance where the model fits the data) only fill a tiny volume. This is where the MCMC approach, based on the Bayesian statistics, is superior to a grid approach. As in the grid approach, one end-product of the analysis is the χ^2 surface, but with a more efficient sampling of the region of interest. Moreover, as opposed to classical statistics, which is based on the construction of estimators of the parameters, Bayesian statistics assumes the unknown parameters to be random variables. As such, their full distribution-the so-called conditional probability-density function (PDF)given some experimental data (and some prior density for these parameters) can be generated.

4 Bayesian Inference

Bayesian inference is one of the two dominant approaches to statistical inference. It expresses the conditional probability, or 'posterior probability', of an event A after B is observed in terms of the 'prior probability' of A, prior probability of B, and the conditional probability of B given A, denoted by B|A.

4.1 Model-based Bayes' theorem

Bayes' theorem provides an expression for the conditional probability of A given B, that is given by

$$P(A|B) = \frac{P(B|A)\ P(A)}{P(B)} \tag{22}$$

For model-based Bayesian inference, B is replaced with observations 'data', A with parameter set Θ, and probabilities P with densities p. The denominator is dropped, which changes the

relation from equal to 'proportional to', $\propto$. The model-based form is

$$p(\Theta|data) \propto p(data|\Theta)\ p(\Theta) \tag{23}$$

Our aim is to determine the conditional probability density function(PDF) of the parameters given the data, $p(\Theta|data)$. This so-called **posterior** probability quantifies the change in the degree of belief one can have in the parameter set $\Theta(\equiv \rho_{DM\circ}, r_S, \rho_{b0}, r_b, \Sigma_\circ, R_d$ in our study) of the model in the light of the data. This theorem links the posterior probability to the **likelihood** of the data $\mathcal{L}(\Theta) \equiv p(data|\Theta)$ and the so-called **prior** probability, $p(\Theta)$, indicating the degree of belief one has before observing the data. To extract information about a single parameter, $\Theta^{(\alpha)}$, the posterior density is integrated over all other parameters $\Theta^{(k\neq\alpha)}$ in a procedure called marginalisation. Finally, by integrating the individual posterior PDF further, we are able to determine the expectation value, confidence level, or higher order mode of the parameter $\Theta^{(\alpha)}$.

4.2 Motivation for MCMC

Above illustrates the technical difficulty of Bayesian parameter estimates: determining the individual posterior PDF requires a high-dimensional integration of the overall posterior density. Thus, an efficient sampling method for the posterior PDF is mandatory. For models of more than a few parameters, regular grid-sampling approaches are not applicable and statistical techniques are required (Cowan 1997).

Among these techniques, MCMC algorithms have been fully tried and tested for Bayesian parameter inference (MacKay 2003; Neal 1993). MCMC methods explore any target distribution given by a vector of parameters $p(\Theta)$, by generating a sequence of $\mathbf{n}$ points from the parameter space which is called a chain

$$\{\Theta_i\}_{i=1\cdots n} = \{\Theta_1, \Theta_2 \cdots \Theta_n\} \tag{24}$$

Each Θ_i is a vector of say, $\mathbf{m}$(=6 in our study) components. In addition, the chain is Markovian in the sense that the distribution of Θ_{n+1} is influenced entirely by the value of Θ_n . MCMC algorithms are developed so that the time spent by the Markov chain in a region of the parameter space is proportional to the target PDF value in this region. Hence, from such a chain, one can obtain an independent sampling of the PDF. The target PDF as well as all marginalised PDF are estimated by counting the number of samples within the related region of parameter space.

5 Affine invariant ensemble sampler

In general, MCMC sampling can be very time consuming in practical problems when the likelihood function is hard to evaluate numerically. Therefore, in our study we use more recent MCMC algorithms such as the one by Goodman and Weare(GW)(2010) instead of MH(Metropolis-Hastings algorithm). We therefore outline the algorithm and its implementation by Foreman-Mackey (2012).[6]

5.1 Algorithm by Goodman and Weare

Unlike updating a single position during the course of the sampling as in MH, GW uses an ensemble of walkers which are spread on the parameter space of the target distribution. At

each iteration, the walkers are randomly assigned to a partner walker chosen from the ensemble and a random point on a line connecting their positions is proposed as the next step. More formally, let Θ_t^i denote the position of walker i after t iterations. When updating this position to Θ_{t+1}^i , we pick another walker Θ_t^j at random with $j \neq i$, sample a value z from the fixed distribution

$$q(z) = \begin{cases} \frac{1}{\sqrt{z}} & if z \in \left[\frac{1}{a}, a\right] \\ 0 & otherwise \end{cases} \tag{25}$$

with tuning parameter a and propose the position $\Theta\prime = \Theta_t^j + z(\Theta_t^k - \Theta_t^j)$. After evaluating the target distribution p at the proposed position, we accept the step if

$$z^{d-1}\frac{p(\Theta\prime)}{p(\Theta_t^i)} > r \tag{26}$$

with r being a random number from [0 , 1] and d the dimension of p. GW is affine invariant, i.e. invariant under linear transformations of the target distribution. This implies in particular that the sampler is not sensitive to the scales of the parameters and does not depend on the covariances of the target distribution.

5.2 Emcee Hammer

The algorithm by Goodman and Weare (2010) was slightly altered and implemented as the Python module emcee by Foreman- Mackey et al. (2012). In this implementation, the algorithm does not update the walkers serially but instead divides them into two subgroups and updates all of the walkers from one subgroup at a time, using the other half of the walkers as their references.

5.3 CosmoHammer: Implementation of emcee Hammer

Arkert et.al[8] developed a Python framework called CosmoHammer for the estimation of cosmological parameters. Their code embeds the Python package emcee by Foreman-Mackey et al. (2012) and gives the user the possibility to plug in modules for the computation of any desired likelihood. The major goal of the software is to reduce the complexity when one wants to extend or replace the existing computation by modules which fit the user's needs as well as to provide the possibility to easily use large scale computing environments.

5.4 Internal design

The internal design of CosmoHammer separates parameter space exploration, theory prediction and likelihood computation. This makes it easy to extend or replace these modules by new algorithms. The concept of CosmoHammer divides the modules in two logical groups: modules for the computation of the likelihood and core modules. The core modules produce information like the rotation curve or other theory predictions for the likelihood modules. The individual core modules can be combined in an instance of the LikelihoodComputationChain module (Fig.[4]). The chain stores the modules and initialises them in the right order. Furthermore, it ensures that the sampled parameters stay within physically motivated bounds during the sampling process. The modules in the LikelihoodComputationChain communicate via the ChainContext in which arbitrary data can be stored and retrieved. This minimises the dependencies between the individual modules and ensures that they can be replaced without the need to change or extend CosmoHammer.

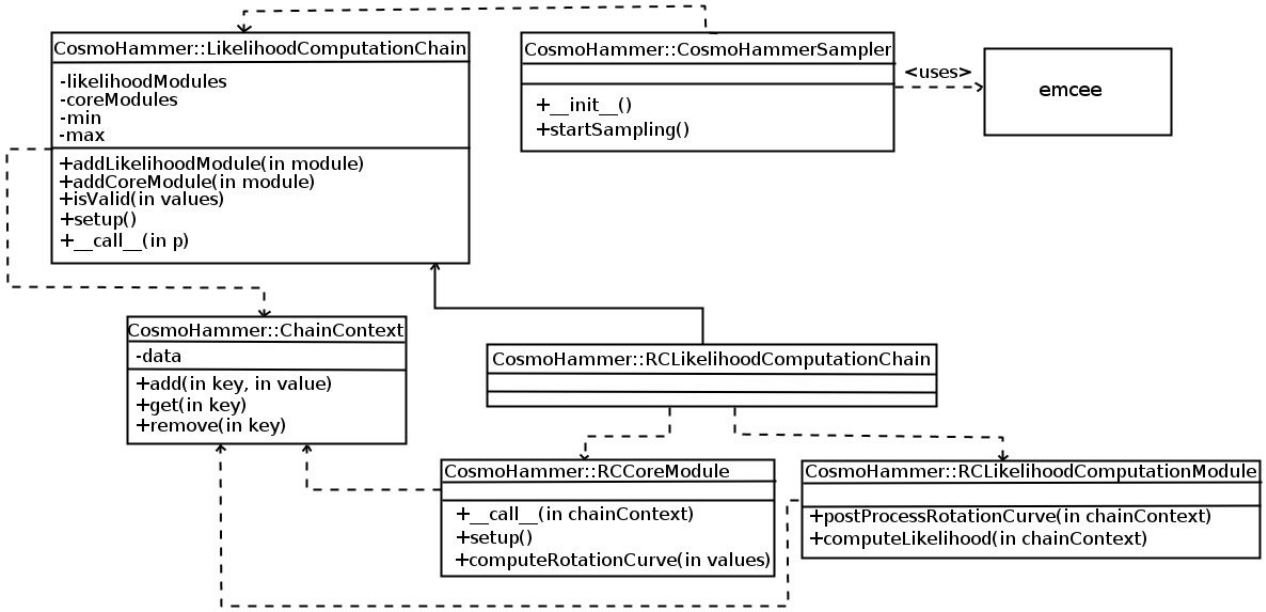

Figure 4: Class diagram of CosmoHammer's main architecture that we used

6 Results

6.1 MCMC run from recently compiled RC data

We present our results from the implementation of CosmoHammer in fitting the rotation curve data. For the observational data, we use a recently compiled set of RC data[9] that extends to Galactocentric distances well beyond the visible edge of the Galaxy. This data set corresponds to a choice of the Local Standard of Rest (LSR) set to $(R_0, v_{c,\circ}) = (8.0 \text{ kpc}, 200\text{kms}^{-1})$.

For priors on the free parameters involved, we have taken the following ranges of the relevant parameters based on currently available observational knowledge

Parameter	Range
$\rho_{DM\circ}$ $(GeV\ cm^{-3})$	$[0.1 - 0.5]$
r_s (kpc)	$[0.01 - 100.]$
$\rho_{b0}(\times 4.2 \times 10^2 M_\circ\ pc^{-3})$	$[0.1 - 2.]$
$r_b(\times 0.103\ kpc)$	$[0.01 - 2.]$
$\Sigma_\circ$ $(M_\circ\ pc^{-2})$	$[35. - 58]$
R_d (kpc)	$[1.7 - 3.5]$

Priors on the model parameters

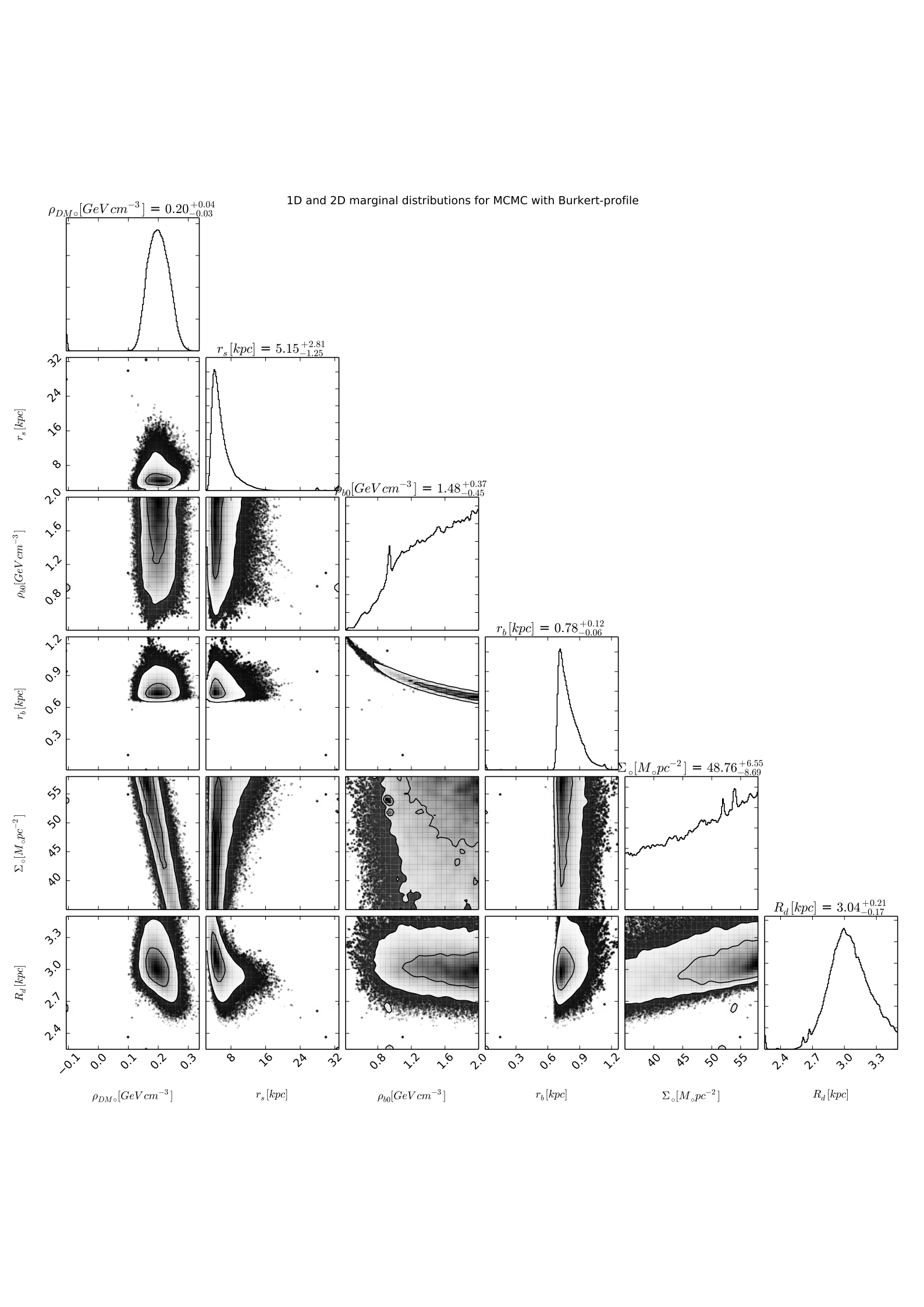
1D and 2D marginal distributions for MCMC with Burkert-profile
$\rho_{DM\circ}[GeV\,cm^{-3}] = 0.20^{+0.04}_{-0.03}$
$r_s\,[kpc] = 5.15^{+2.81}_{-1.25}$
$\rho_{b0}[GeV\,cm^{-3}] = 1.48^{+0.37}_{-0.45}$
$r_b\,[kpc] = 0.78^{+0.12}_{-0.06}$
$\Sigma_\circ[M_\circ pc^{-2}] = 48.76^{+6.55}_{-8.69}$
$R_d\,[kpc] = 3.04^{+0.21}_{-0.17}$
$\rho_{DM\circ}[GeV\,cm^{-3}]$
$r_s\,[kpc]$
$\rho_{b0}[GeV\,cm^{-3}]$
$r_b\,[kpc]$
$\Sigma_\circ[M_\circ pc^{-2}]$
$R_d\,[kpc]$

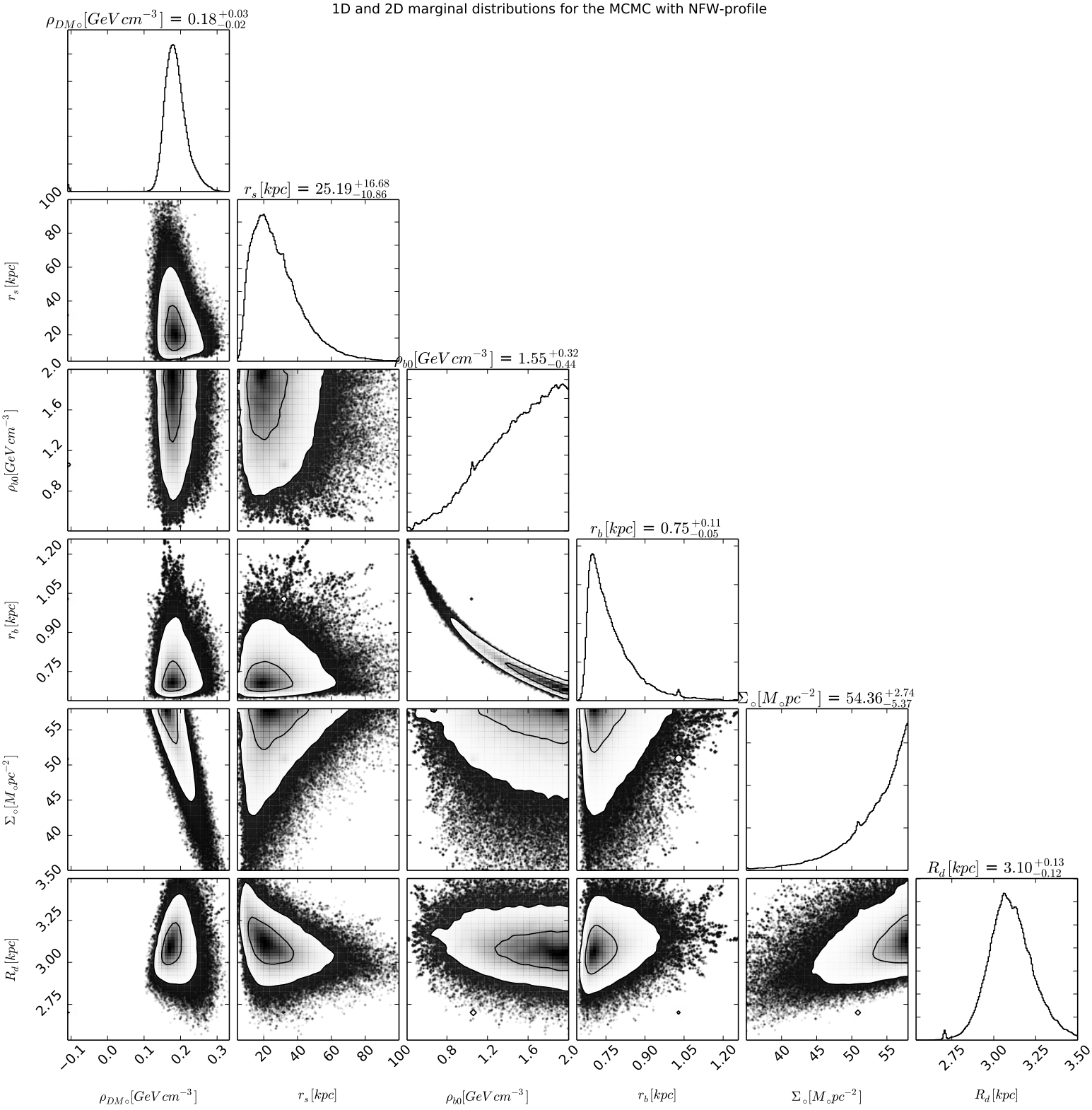
1D and 2D marginal distributions for the MCMC with NFW-profile
$\rho_{DM\circ}[GeV\,cm^{-3}] = 0.18^{+0.03}_{-0.02}$
$r_s\,[kpc] = 25.19^{+16.68}_{-10.86}$
$\rho_{b0}[GeV\,cm^{-3}] = 1.55^{+0.32}_{-0.44}$
$r_b\,[kpc] = 0.75^{+0.11}_{-0.05}$
$\Sigma_\circ[M_\circ pc^{-2}] = 54.36^{+2.74}_{-5.37}$
$R_d\,[kpc] = 3.10^{+0.13}_{-0.12}$
$\rho_{DM\circ}[GeV\,cm^{-3}]$
$r_s\,[kpc]$
$\rho_{b0}[GeV\,cm^{-3}]$
$r_b\,[kpc]$
$\Sigma_\circ[M_\circ pc^{-2}]$
$R_d\,[kpc]$

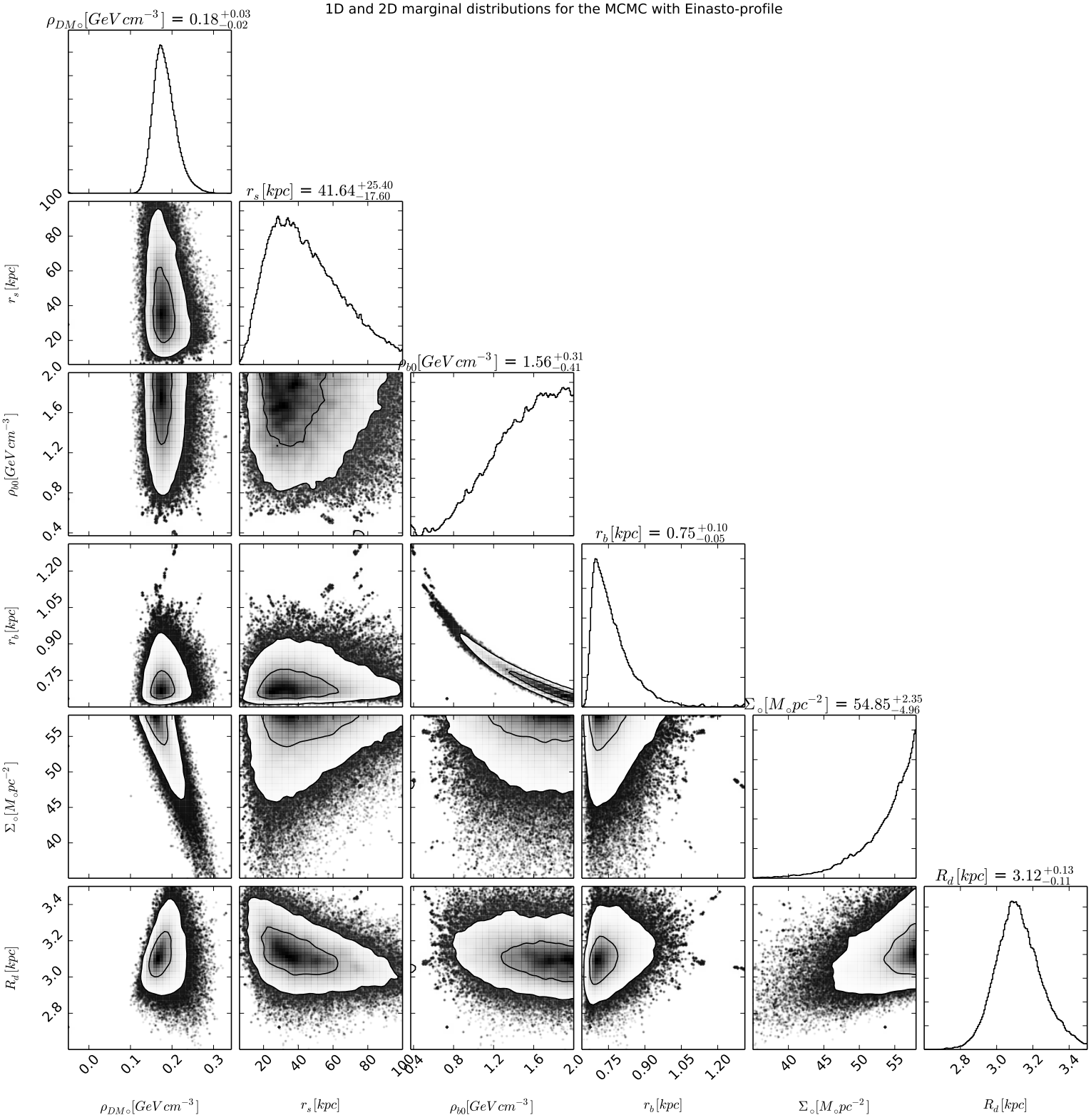
1D and 2D marginal distributions for the MCMC with Einasto-profile
$\rho_{DM\circ}[GeV\,cm^{-3}] = 0.18^{+0.03}_{-0.02}$
$r_s[kpc] = 41.64^{+25.40}_{-17.60}$
$\rho_{b0}[GeV\,cm^{-3}] = 1.56^{+0.31}_{-0.41}$
$r_b[kpc] = 0.75^{+0.10}_{-0.05}$
$\Sigma_\circ[M_\circ pc^{-2}] = 54.85^{+2.35}_{-4.96}$
$R_d[kpc] = 3.12^{+0.13}_{-0.11}$
$\rho_{DM\circ}[GeV\,cm^{-3}]$
$r_s[kpc]$
$\rho_{b0}[GeV\,cm^{-3}]$
$r_b[kpc]$
$\Sigma_\circ[M_\circ pc^{-2}]$
$R_d[kpc]$

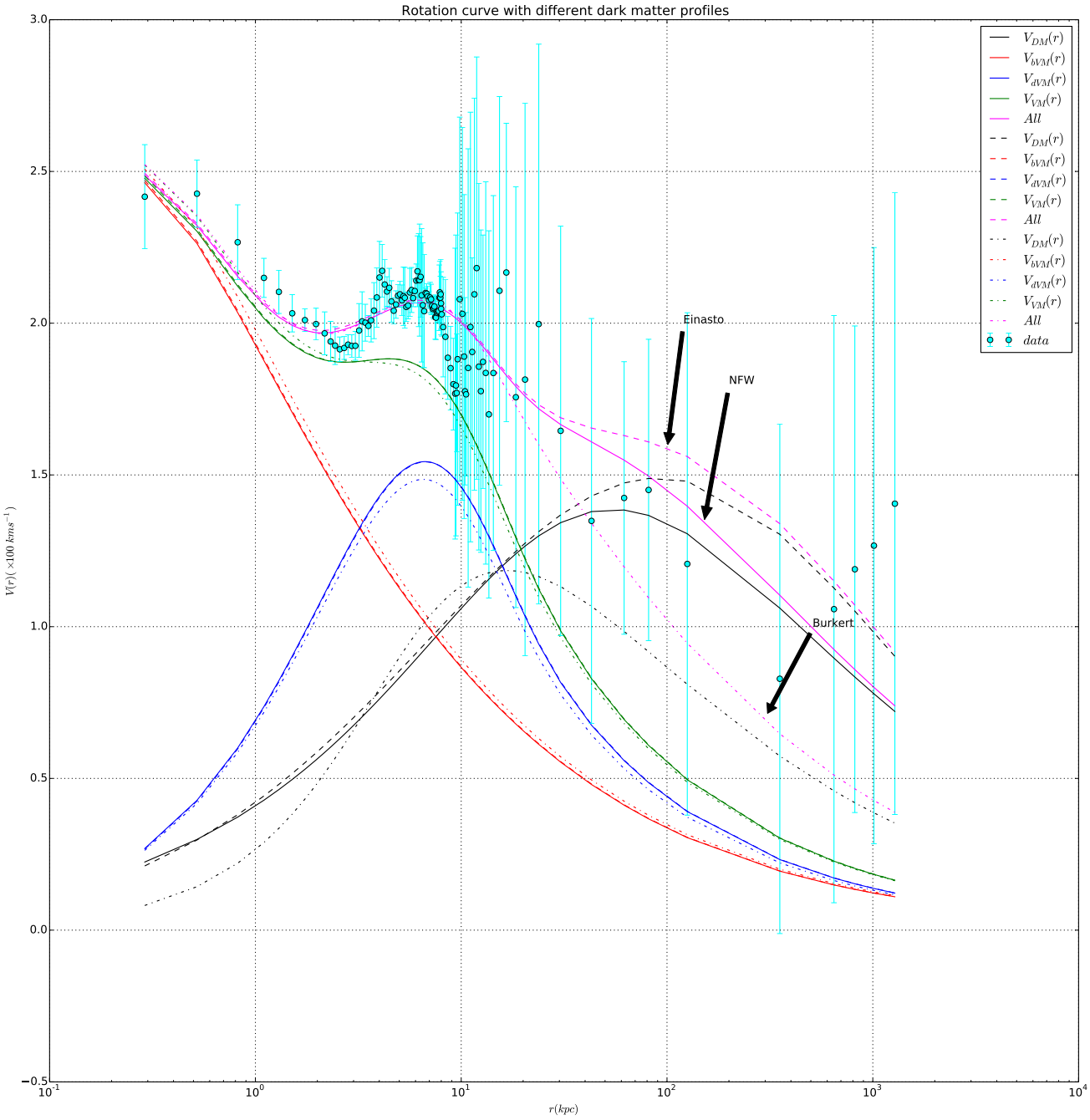
Rotation curve with different dark matter profiles
Einasto
NFW
Burkert
$V_{DM}(r)$
$V_{bVM}(r)$
$V_{dVM}(r)$
$V_{VM}(r)$
All
$data$
$V(r)(\times 100\,kms^{-1})$
$r(kpc)$

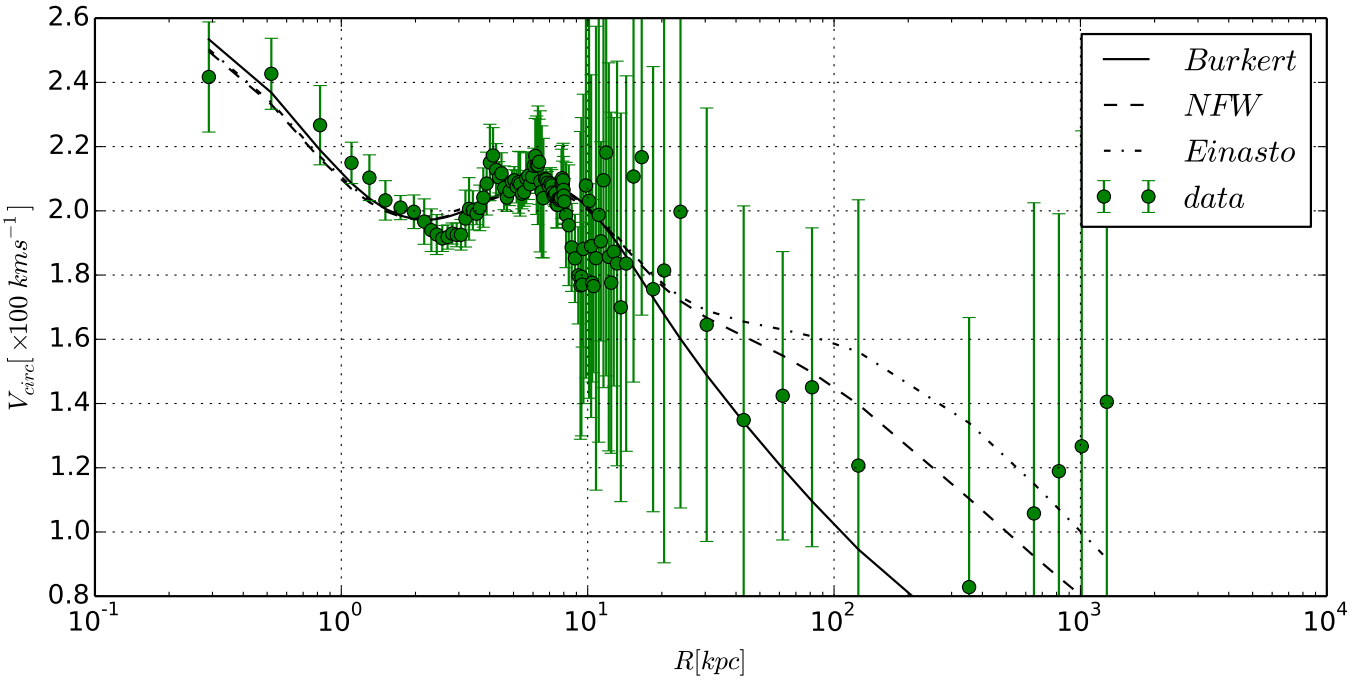
Burkert
NFW
Einasto
data
$V_{circ}[\times 100\ kms^{-1}]$
$R[kpc]$

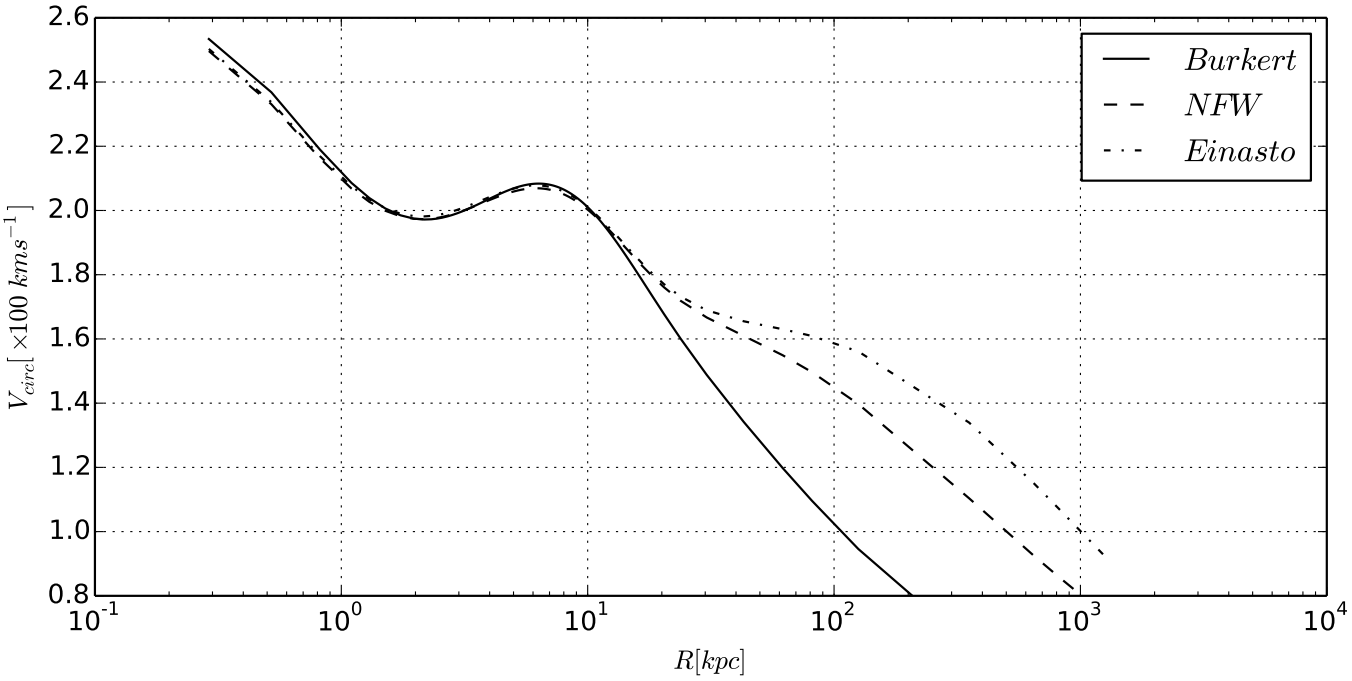
Burkert
NFW
Einasto
$V_{circ}[\times 100\ kms^{-1}]$
$R[kpc]$

6.2 Tabulated results

$Burnin - iter.$	$Sample - iter.$	$Parameters$	NFW	$Burkert$	$Einasto$
1000	2000	$\rho_{DM\circ}$	$0.18^{+0.03}_{-0.02}$	$0.20^{+0.04}_{-0.03}$	$0.18^{+0.03}_{-0.02}$
		r_s	$25.19^{+16.68}_{-10.86}$	$5.15^{+2.81}_{-1.25}$	$40.77^{+25.52}_{-16.81}$
		ρ_{b0}	$1.55^{+0.32}_{-0.44}$	$1.48^{+0.37}_{-0.45}$	$1.54^{+0.32}_{-0.45}$
		r_b	$0.75^{+0.11}_{-0.05}$	$0.78^{+0.12}_{-0.06}$	$0.75^{+0.11}_{-0.05}$
		$\Sigma_\circ$	$54.36^{+2.74}_{-5.37}$	$48.76^{+6.55}_{-8.69}$	$54.81^{+2.39}_{-4.72}$
		R_d	$3.10^{+0.13}_{-0.12}$	$3.04^{+0.21}_{-0.17}$	$3.12^{+0.13}_{-0.12}$
1500	1000	$\rho_{DM\circ}$	$0.18^{+0.03}_{-0.02}$	$0.20^{+0.04}_{-0.04}$	$0.18^{+0.03}_{-0.02}$
		r_s	$25.21^{+16.61}_{-10.56}$	$5.02^{+2.46}_{-1.15}$	$40.12^{+24.38}_{-16.74}$
		ρ_{b0}	$1.54^{+0.32}_{-0.44}$	$1.44^{+0.37}_{-0.44}$	$1.56^{+0.31}_{-0.42}$
		r_b	$0.75^{+0.10}_{-0.05}$	$0.78^{+0.12}_{-0.07}$	$0.75^{+0.10}_{-0.05}$
		$\Sigma_\circ$	$54.39^{+2.71}_{-5.49}$	$47.44^{+7.58}_{-8.05}$	$54.80^{+2.37}_{-4.60}$
		R_d	$3.10^{+0.14}_{-0.12}$	$3.04^{+0.21}_{-0.17}$	$3.12^{+0.13}_{-0.11}$
2000	1000	$\rho_{DM\circ}$	$0.19^{+0.03}_{-0.02}$	$0.20^{+0.04}_{-0.04}$	$0.18^{+0.03}_{-0.02}$
		r_s	$24.74^{+16.15}_{-9.83}$	$5.08^{+2.69}_{-1.17}$	$38.82^{+24.00}_{-15.89}$
		ρ_{b0}	$1.52^{+0.33}_{-0.44}$	$1.49^{+0.35}_{-0.43}$	$1.55^{+0.32}_{-0.45}$
		r_b	$0.75^{+0.11}_{-0.06}$	$0.77^{+0.11}_{-0.06}$	$0.74^{+0.11}_{-0.05}$
		$\Sigma_\circ$	$54.37^{+2.71}_{-5.84}$	$48.15^{+7.07}_{-8.43}$	$54.83^{+2.35}_{-4.81}$
		R_d	$3.10^{+0.13}_{-0.12}$	$3.04^{+0.21}_{-0.18}$	$3.12^{+0.14}_{-0.12}$

Mean and standard deviation of the parameters sampled by CosmoHammer for different Dark Matter profiles

6.3 MCMC run from mock RC data

Here we present our results from the MCMC run on the mock RC data. This data was obtained by reducing the error bar on the previous RC data to 5%. These errors are more like the mock errors for the current mission called GAIA. Current observations cannot differentiate between different models of DM distribution, we show that upcoming data, from mission like GAIA, will be able to nail down the DM distribution with exquisite accuracy. In the next page we show the results from MCMC run with NFW-profile and for extended parameter range. We also show the fit to the mock data with the most likely values obtained in this run.

Parameter	Range
$\rho_{DM\circ}$ $(GeV\ cm^{-3})$	$[0.1 - 0.5]$
r_s (kpc)	$[0.01 - 100.]$
$\rho_{b0}(\times 4.2 \times 10^2 M_\circ\ pc^{-3})$	$[0.1 - 4.]$
$r_b(\times 0.103\ kpc)$	$[0.01 - 2.]$
$\Sigma_\circ$ $(M_\circ\ pc^{-2})$	$[35. - 90.]$
R_d (kpc)	$[1.7 - 4.]$

Extended priors on the model parameters for future data runs

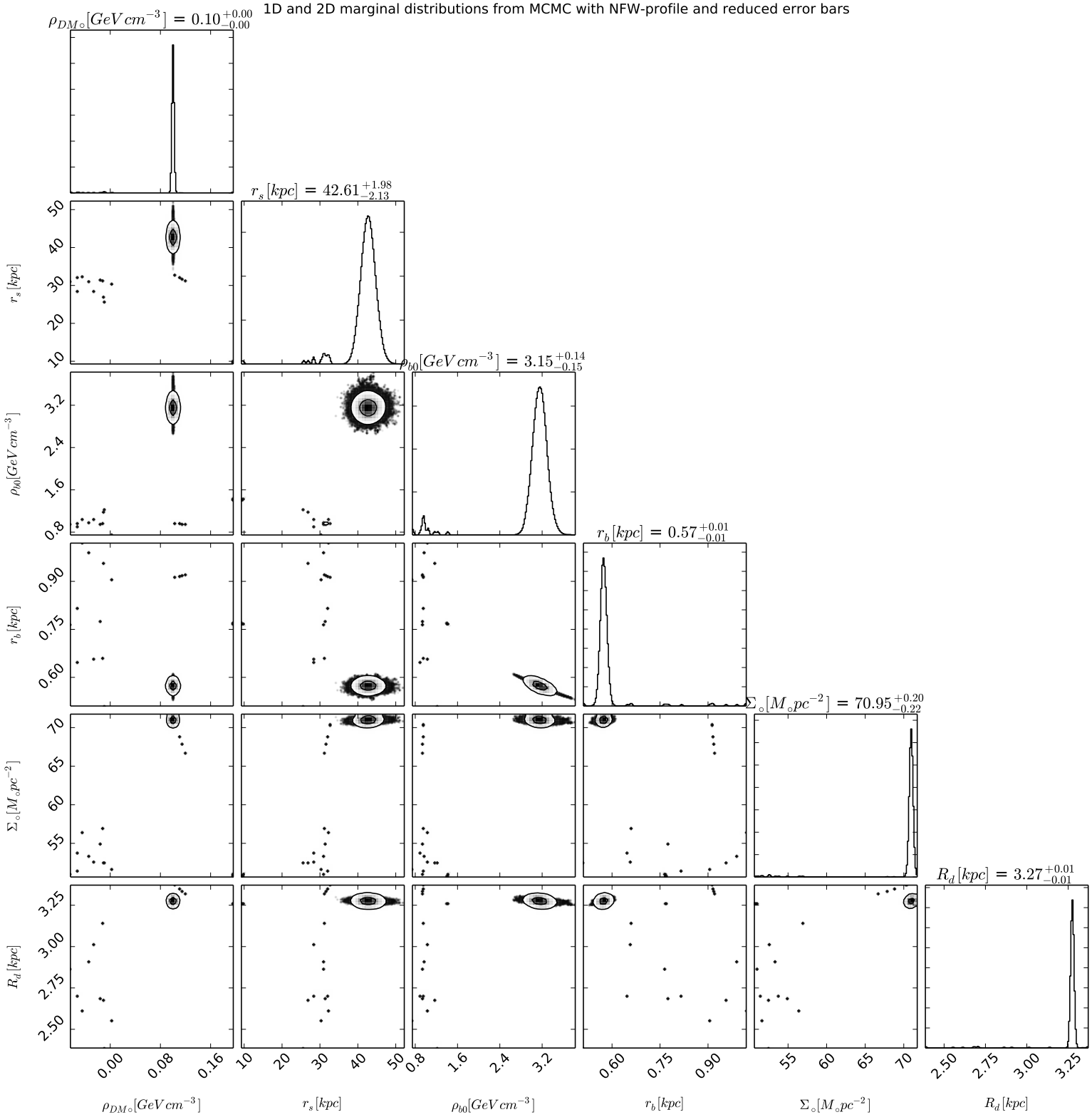
1D and 2D marginal distributions from MCMC with NFW-profile and reduced error bars
$\rho_{DM\circ}[GeV\,cm^{-3}] = 0.10^{+0.00}_{-0.00}$
$r_s\,[kpc] = 42.61^{+1.98}_{-2.13}$
$\rho_{b0}[GeV\,cm^{-3}] = 3.15^{+0.14}_{-0.15}$
$r_b\,[kpc] = 0.57^{+0.01}_{-0.01}$
$\Sigma_\circ[M_\circ pc^{-2}] = 70.95^{+0.20}_{-0.22}$
$R_d\,[kpc] = 3.27^{+0.01}_{-0.01}$
$\rho_{DM\circ}[GeV\,cm^{-3}]$
$r_s\,[kpc]$
$\rho_{b0}[GeV\,cm^{-3}]$
$r_b\,[kpc]$
$\Sigma_\circ[M_\circ pc^{-2}]$
$R_d\,[kpc]$

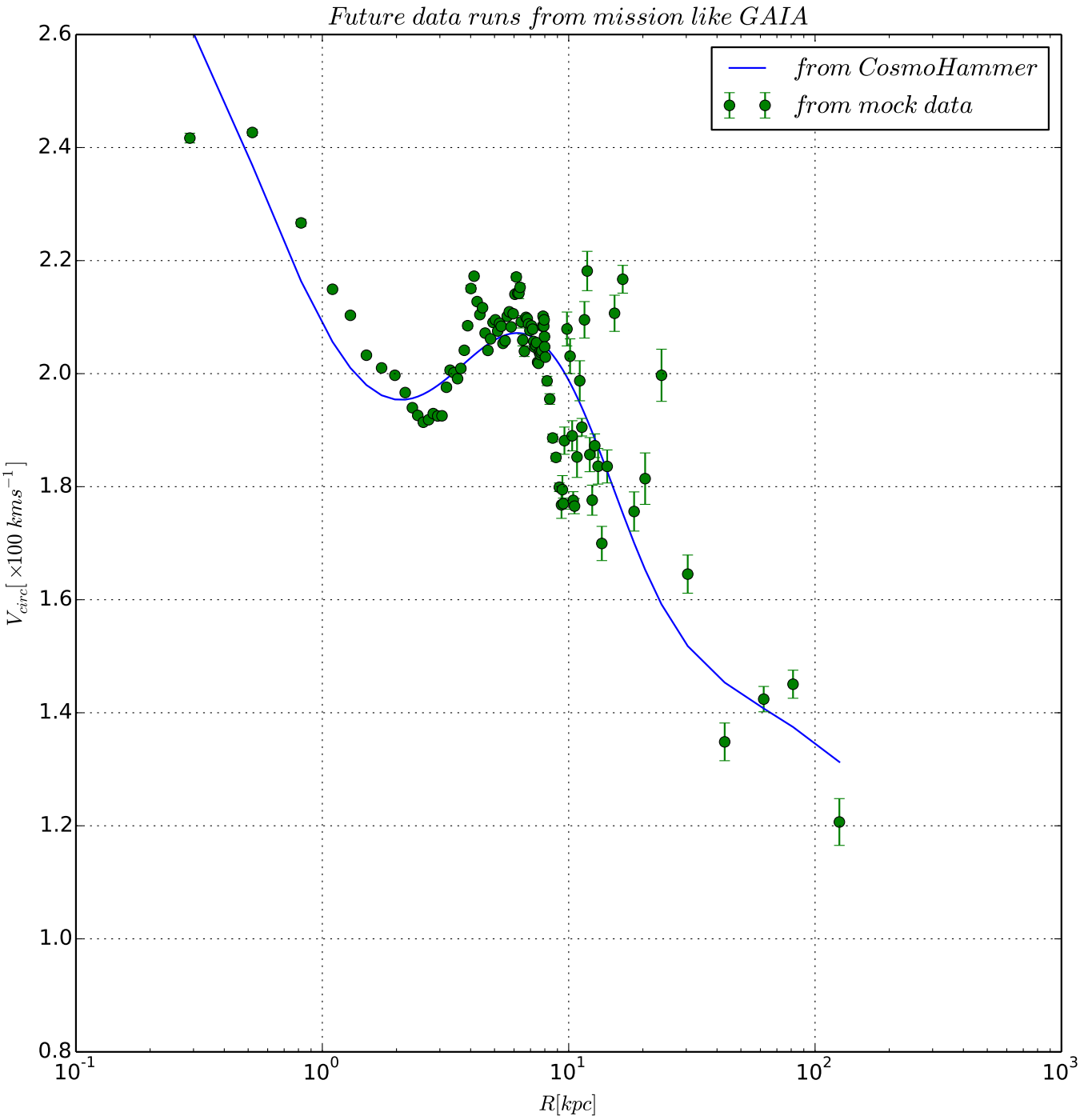
Future data runs from mission like GAIA
from CosmoHammer
from mock data
$V_{circl}[\times 100\ kms^{-1}]$
$R[kpc]$
2.6
2.4
2.2
2.0
1.8
1.6
1.4
1.2
1.0
0.8
10^{-1}
10^{0}
10^{1}
10^{2}
10^{3}

6.4 Tabulated result

$Parameter$	$Value$
$\rho_{DM\circ}$	$0.10^{+0.00}_{-0.00}$
r_s	$42.61^{+1.98}_{-2.13}$
ρ_{b0}	$3.15^{+0.14}_{-0.15}$
r_b	$0.57^{+0.01}_{-0.01}$
$\Sigma_\circ$	$70.95^{+0.20}_{-0.22}$
R_d	$3.27^{+0.01}_{-0.01}$

Parameter values from the MCMC run on the extended parameter range for future data runs

7 Summary

In cosmological applications, fast and efficient MCMC methods are crucial whenever the sampling has to be repeated numerous times and evaluating the target distribution is computationally expensive. In our study we used emcee sampler by Foreman-Mackey et al. (2012) which turned out to be a good choice as it not only requires no tuning of the algorithm in general but is also affine invariant, i.e. invariant under linear transformations of the target distribution. This implies in particular that the sampler is not sensitive to the scales of the parameters and does not depend on the covariances of the target distribution.
By the improvement of the parameter constraints(the priors), the central values have shifted because of lesser priors , i.e larger range. This hints towards tighter constraints on the parameters. The upcoming data from mission like GAIA will be able to nail down the dark matter distribution more accurately.

Bibliography

[1] Rubin, V. C., Thonnard, N., and Ford, W. K., Jr., 1978, ApJ 225 L107-L111

[2] V. Rubin, N. Thonnard, W. K. Ford, Jr, (1980). "Rotational Properties of 21 Sc Galaxies with a Large Range of Luminosities and Radii from NGC 4605 (R=4kpc) to UGC 2885 (R=122kpc)". Astrophysical Journal 238: 471.

[3] M. Persic, P. Salucci, F. Stel (1996). "The universal rotation curve of spiral galaxies - I. The dark matter connection". Monthly Notices of the Royal Astronomical Society 281 (1): 2747.

[4] J. Caldwell and J. Ostriker, ApJ 251 (1981) 61; K. Kuijken and G. Gilmore, MNRAS 239 (1989) 571; ibid. 239 (1989) 605; ibid. 239 (1989) 651; ApJ L9 (1991) 367.

[5] Duric, Nub (2004) Advanced Astrophysics, Cambridge University Press, Cambridge, UK

[6] Foreman-Mackey, D., Hogg, D.W., Lang, D., Goodman, J., 2012. emcee: the MCMC hammer

[7] Akeret, J; Seehars, S.; Amara, A.; Refregier, A.; Csillaghy, A., 2013, A&C, 2, 27 [http://www.cosmology.ethz.ch/research/software-lab/cosmohammer.html]

[8] J. Akeret et al. Astronomy and Computing 2 (2013) 2739

[9] Y. Sofue, PASJ 64 (2012) 75 [arXiv:1110.4431]